THE CHEMICAL PHYSICS OF SOLID SURFACES

EDITED BY

D.A. KING

B.Sc., Ph.D. (Rand), Sc.D. (East Anglia), F.R.S.
1920 Professor of Physical Chemistry,
University of Cambridge

AND

D.P. WOODRUFF

B.Sc. (Bristol), Ph.D., D.Sc. (Warwick)
Professor of Physics,
University of Warwick

VOLUME 8

GROWTH AND PROPERTIES OF ULTRATHIN EPITAXIAL LAYERS

ELSEVIER

AMSTERDAM – LAUSANNE – NEW YORK – OXFORD – SHANNON – TOKYO
1997

Growth and Properties of Ultrathin Epitaxial Layers
D.A. King and D.P. Woodruff, editors.

Chapter 9

Structure and electronic properties of ultrathin oxide films on metallic substrates

H. Kuhlenbeck and H.-J. Freund

Fritz-Haber-Institut der Max-Planck-Gesellschaft, Abteilung Chemische Physik, Faradayweg 4-6, 14195 Berlin, Germany

This chapter will deal with the properties of ultrathin oxide layers on different substrates. We will discuss different modes of preparation, the surface geometry of the respective oxide films and their electronic properties. The focus will be put onto the systems NiO(100)/Ni(100), NiO(111)/Ni(111), Cr_2O_3(0001)/Cr(110) and Al_2O_3(111)/NiAl(110), that are prepared by oxidation of metal or alloy single crystals in an oxygen atmosphere at elevated temperature. We will also discuss systems where the oxide film is prepared by oxidation of a metal which is evaporated onto an inert substrate.

1. INTRODUCTION

Oxides are interesting materials from different points of view. Seen from the viewpoint of technology the fields of catalysis, corrosion, semiconductor technology and high temperature superconductivity are to be listed although the technological breakthrough in the latter discipline is still to come. We also note that ceramic materials which are used for numerous applications are oxidic in nature.

Using surface science methods one may try to get information on the properties of the surfaces of oxides and their interaction with other materials like adsorbed gases. The latter aspect is important for the field of catalysis.

Many studies on oxide surfaces have been performed since the event of surface science; especially in the last ten years several groups all around the world have begun to study different aspects of the properties of oxidic surfaces. In the beginning these groups mainly concentrated on the electronic and geometric properties of clean surfaces [1, 2, 3]. From the joint theoretical and experimental efforts our knowledge of oxide surfaces has rapidly developed. Another step is to study the interaction of oxides with other materials, especially

adsorbed gases [4]. Founded knowledge about the interaction of adsorbates with the surface, the modification of their properties due to adsorbate-surface interactions and interactions between adsorbed molecules is an important ingredient for an understanding of many technologically important catalytic processes. Real heterogeneous catalysts often consist of metal particles finely dispersed on an oxidic support[5]. Therefore the interaction of oxide surfaces with metals is another important aspects of many studies [6, 7].

There are different ways to study oxide materials. One involves the investigation of powder samples with sometimes rather undefined structure[8]. Often the experiments are performed at ambient pressure conditions. This approach is mainly used in catalytic studies but there is the disadvantage that it is often not easy to understand the results from a microscopic point of view since the samples are too complicated in structure and the ambient pressure conditions do not allow the in situ application of electron spectroscopy. In another approach oxide single crystals are investigated [2]. Such surfaces may be obtained by cleaving a single crystal in vacuo or by cutting a piece from a single crystal rod and polishing it. Especially cleaved single crystal surfaces may be prepared with low defect density so that the experimentalist deals with a very well defined system (this advantage is usually less pronounced for polished surfaces) so that the experimental results are often easier to understand. The main problem here is that such systems tend to charge when electron spectroscopy is applied and that defined heating of the samples is problematic since the heat conductivity of oxides is typically small. Charging is especially found at low temperatures since at these temperatures the movement of charge carriers is frozen in [9]. However, low temperatures are important for adsorption studies.

The third approach which will be in the focus of this chapter is to study thin oxide films[4, 10]. These are often prepared by oxidation of a metal single crystal but other methods of preparation may also be applied. Cooling and heating are unproblematic and usually no charging occurs even at low temperature so that electron spectroscopy may be applied. Also, it is possible to prepare surfaces which may not be obtained by cleaving since their surface energy is too high.

We shall present results for several different oxide systems, i.e. NiO(100)/Ni(100), NiO(111)/Ni(111), NiO(111)/Au(111), Cr_2O_3(0001)/Cr(110) and Al_2O_3(111)/NiAl(110). The preparation and the structure of the films as well as their electronic properties will be in the focus of the discussion. We will also discuss the stabilization of polar surfaces and a few aspects of the interaction with adsorbates.

2. PREPARATION OF THIN OXIDE FILMS

There are three commonly applied methods of oxide film preparation which are depicted in Fig. 1. One way is to simply oxidize metal single crystals by exposition to oxygen at elevated temperature as schematically shown in Fig. 1a [4]. Oxide films may also be grown by oxidation of alloy surfaces as depicted in Fig. 1b [11, 12]. If, for instance, the oxide of metal B is thermodynamically much more stable than that of metal A nearly exclusively the oxide of metal B is formed. This works well for some aluminum alloys because Al_2O_3 is thermodynamically very stable. It may also be favorable to grow an oxide film on a substrate which itself does not play a role in the process of oxide formation as depicted in Fig. 1c [13-17]. This may, for instance, be done by evaporating a metal in an oxygen atmosphere or by oxidizing a metal layer deposited on an

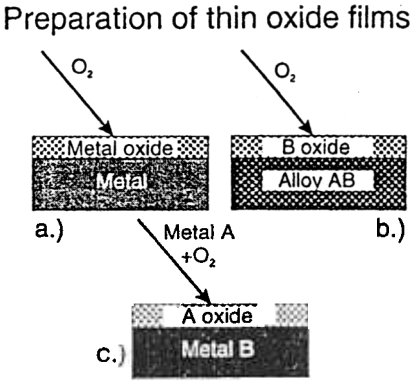

Fig. 1: Three different methods for the preparation of oxide films.

inert substrate. Such a procedure is advantageous if the lattice constant of the oxide does not fit well to that of the respective metal so that the resulting strain induces defects if the film is prepared by oxidation of the respective metal. As a way out one may chose a substrate with a lattice constant that fits well to that of the oxide.

Typical thicknesses of experimentally studied oxide films range from several Ångstrøms to some 10 nanometers. Thicknesses of some nanometers are usually sufficient for the oxide films in order to establish a geometric and electronic structure which is near to that of a massive oxide crystal. At much higher thickness charging may occur.

The qualities of different oxide films may differ strongly. Besides preparation parameters like oxygen pressure, substrate temperature and evaporation rate also some other parameters strongly influence the quality of the resulting film:

I. The mismatch between the lattice constants of substrate and oxide.
If the mismatch is not too large this may simply result in the formation of a strained oxide lattice. Large mismatches on the other hand may lead to incommensurate layers or layers that consist of small islands or crystallites with some type of defective region between them. The general trend is that an increasing lattice mismatch leads to a decreasing film quality. This is an observation that has also been made for other types of thin films.

II. The oxide-substrate interface energy and the oxide surface energy
If these energies are too high one will observe a three dimensional growth of the oxide film, i.e. small three dimensional islands with uncovered substrate regions between them may form (Volmer-Weber-growth). Especially for adsorption experiments this is highly undesirable.

III. Oxygen diffusion into the substrate
At elevated substrate temperature some oxygen of the oxide may diffuse into the bulk of the substrate thereby leading to an unstoichiometric oxide film [18].

IV. The melting point of the substrate
Al_2O_3 films must be annealed at high temperature to establish crystallinity. If this oxide is prepared by oxidation of an aluminum single crystal, ordering of the oxide film by annealing at sufficiently high temperature is impossible because the substrate will melt [11].

The quality of an oxide film depends on all these parameters. Apart from these also the experimental parameters of the preparation influence the quality of the oxide film. Whereas the first set of parameters is given by the physical properties of the oxide and the substrate, the latter one is usually of empirical nature. In the following we will discuss examples for oxide films prepared according to all three preparation methods depicted in Fig. 1.

3. EXPERIMENTAL RESULTS FOR DIFFERENT OXIDE-METAL SYSTEMS

3.1 NiO(100)/Ni(100), NiO(111)/Ni(111) and NiO(111)/Au(111)

3.1.1 Geometric structure

3.1.1.1 NiO(100)/Ni(100)

NiO is probably the most often studied oxide [16-59]. Many groups studied NiO(100) in order to develop a basic understanding of the electronic structure of oxidic materials and it was the one together with MgO(100) which was most often used as a test system for theoretical models [34-51]. In this chapter we will present data obtained for a thin film of NiO(100) on Ni(100). We will

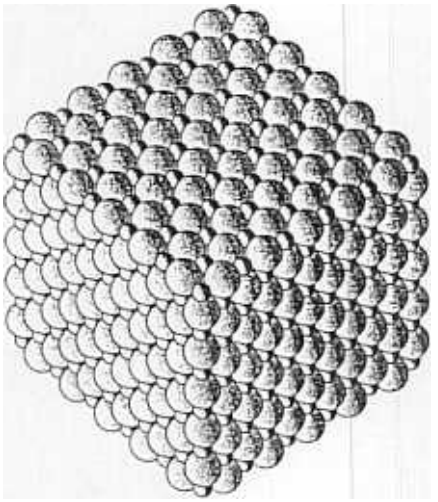

Fig. 2: Structure of a NiO single crystal cube exposing (100) surfaces.

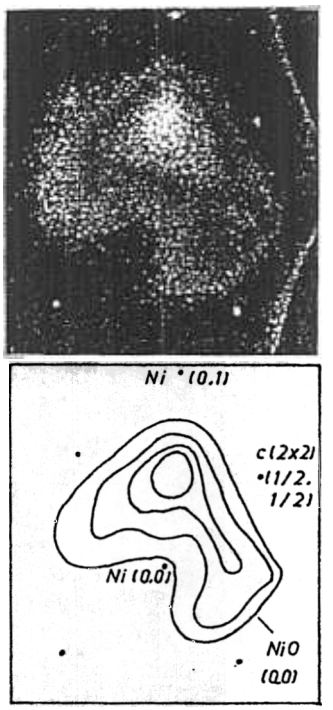

Fig. 3: Top: SPA-LEED pattern of NiO(100) grown by thermal oxidation of Ni(100). Bottom: Schematic drawing of the intensity distribution in the SPA-LEED pattern.

include the electronic structure as well as geometric properties.

The arrangement of ions at the NiO(100) surface is shown in Fig. 2. The lattice type is fcc and the unit cell contains a Ni^{2+} and an O^{2-} ion [60]. NiO(100) films may be grown on Ni(100) by oxidation at elevated temperature (about 300 °C) in an oxygen atmosphere of about $1*10^{-5}$ mbar [19]. The resulting oxide films exhibit a LEED pattern as depicted in Fig. 3 [19, 59]. Some properties of the pattern are remarkable. First: the reflexes are rather broad; second: the center of the (0,0) reflex of the oxide appears to be shifted with respect to that

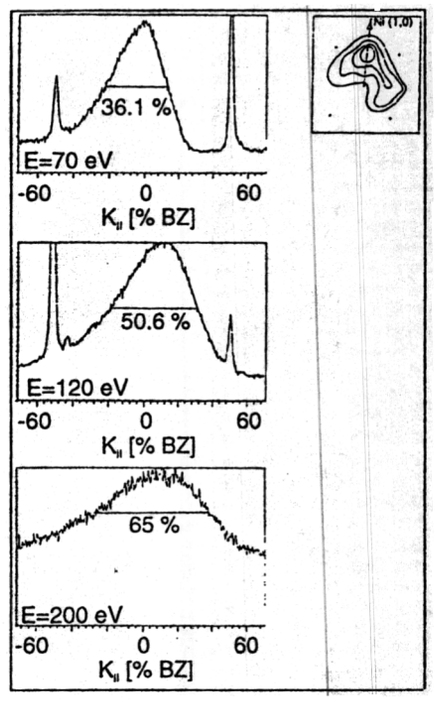

Fig. 4: SPA-LEED line scans through the (0,0) reflex of NiO(100)/Ni(100).

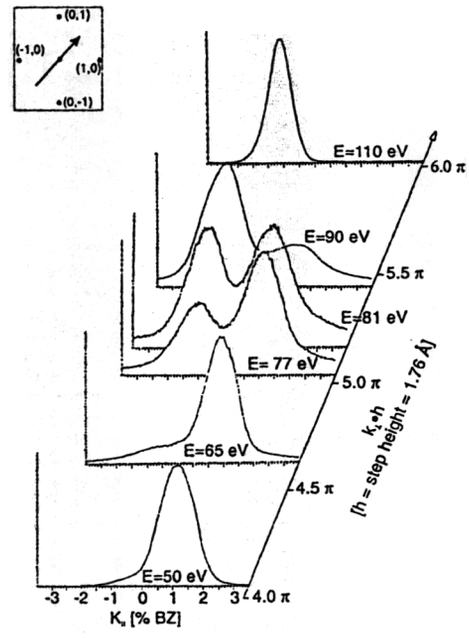

Fig.5: SPA-LEED line scans through the (0,0) reflex of the Ni(100) substrate.

of the substrate; third: there seems to be more than one center of the intensity of the oxide reflex.

The oxide film has been studied using STM and SPA-LEED [19, 59]. Fig. 4 shows a set of SPA-LEED line scans through the oxide (0,0) reflex for different electron energies. It turns out that the FWHM of the reflex varies in k space with varying electron energy whereas the angular spread of the reflex remains approximately constant. This means that the large FWHM of the oxide reflex is not due to defects in the film (at least not in full) but to a tilt of the surface

normal with respect to that of the substrate. This, of course, means that the oxide film consists of tilted crystallites since a tilt of the whole oxide film is hard to imagine.

It still needs to be explained why the (0,0) reflex of the NiO(100) film seems to have more than one center of intensity. In view of the explanations given above this means that there are different possible tilting angles for the NiO crystallites which differ by 90° as is obvious from the intensity distribution of the reflex.

Fig. 5 exhibits a series of line scans through the (0,0) reflex of the Ni(100) substrate taken at different electron energies. One observes energy dependent variations in the reflex profile which are characteristic for an array of steps on the surface with the average step size corresponding to a 1° misorientation of

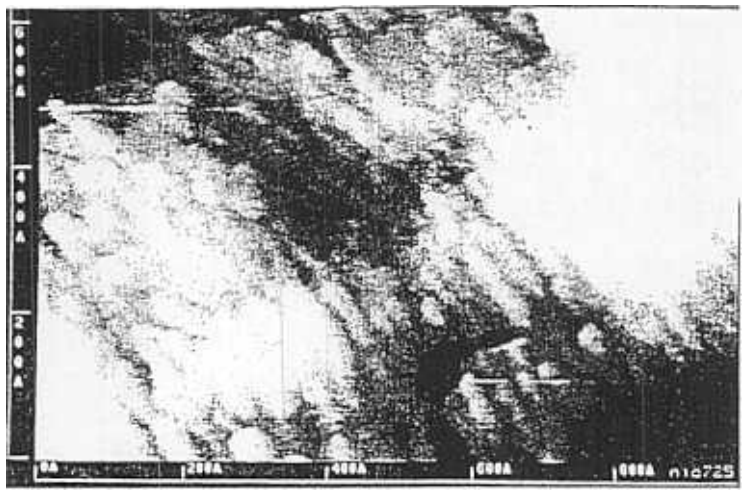

Fig. 6: STM scan of a NiO(100) film.

the surface. These steps descend along [001] as indicated by the data shown in Fig. 5.

Fig. 3 shows that the NiO(100) crystallites tilt only along [011] type directions. But the four possible tilting directions are not equally populated; the crystallites tilt preferably along those [011] type directions that are near to the direction along which the steps on the substrate descend. This indicates that the steps on the substrate play an important role in the oxidation process.

From the SPA-LEED data the average tilting angle and the spread of tilting angles may be estimated to be about 8° and 6°, respectively. The average size of the NiO(100) crystallites as calculated from the SPA-LEED data is about 50 Å. This results is corroborated by STM scans of which one is shown in Fig. 6. The

crystallites of the NiO(100) film are easily discovered. The region between the crystallites most likely consists of defects. From the known data it may be estimated that these defects make up 20 to 25 % of the surface area. The reason for the formation of this type of film structure is most likely the large mismatch of the lattice constants of NiO(100) and Ni(100) which amounts to about 16 %. This leads to strain in the oxide film which breaks up the film into crystallites and most likely also is the reason for the tilt of the crystallites. Finally we note that not in all cases the formations of tilted crystallites has been observed. The tilting seems to occur especially on somewhat misaligned surfaces indicating that a certain density of steps on the surface is needed for tilting to occur. Additionally, the preparation conditions seem to have a certain influence since tilted crystalites are more readily observed on systems which have been annealed at high temperature.

3.1.1.2 NiO(111)/Ni(111)

The surface energy of NiO(111) is higher than that of NiO(100) which means that it can not be prepared by cleavage of a single crystal. However, it can be prepared by oxidation of a Ni(111) single crystal where the film is stabilized by

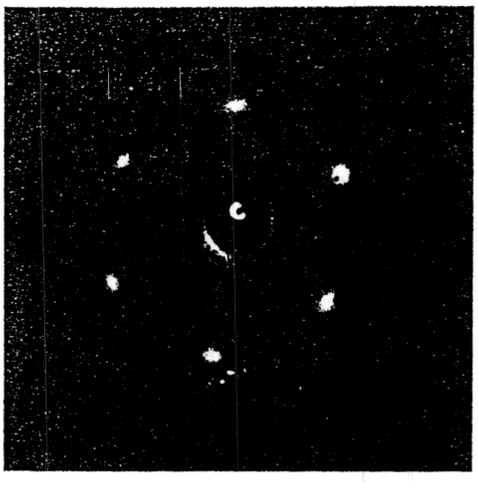

Fig. 7: LEED pattern of NiO(111)/Ni(111).

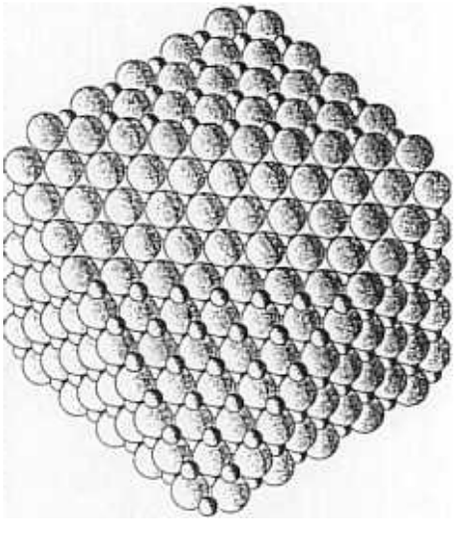

Fig. 8: NiO single crystal cube cut along the (111) surface. Two different terminations of the polar (111) surface are shown. Bottom: Ni^{2+} terminated; top: O^{2-} terminated.

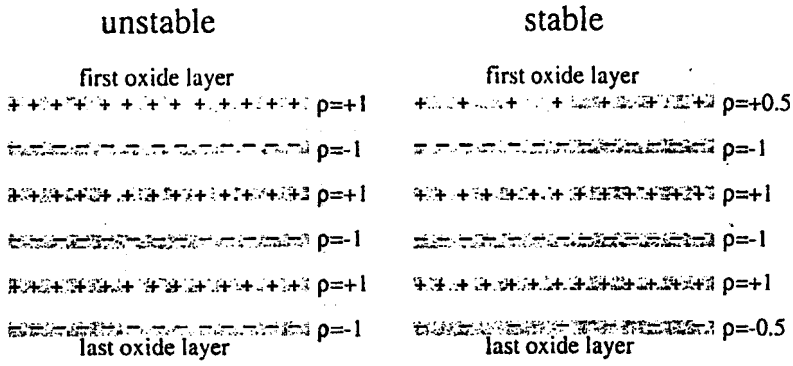

Fig 9: Schematic drawing of a stable and an unstable arrangement of ionic layers at polar surfaces.

the interaction with the substrate [24,58]. Due to the inherent instability of this surface it has to be prepared at somewhat lower temperature as compared to NiO(100)/Ni(100) and the quality of the LEED pattern indicates a large number of defects (Fig. 7) [24, 58].

NiO(111) is a so called polar surface. The first layer of ideally terminated NiO(111) may either consist purely of Ni^{2+} ions or of O^{2-} ions as schematically shown in Fig. 8. Such an arrangement of ions is unstable for energetic reasons since the Madelung potential energy diverges [61, 62]. This may be shown by calculating the potential energy using a model where the ionic layers are approximated by electrically charged planes as shown in Fig. 9 [61, 62]. The

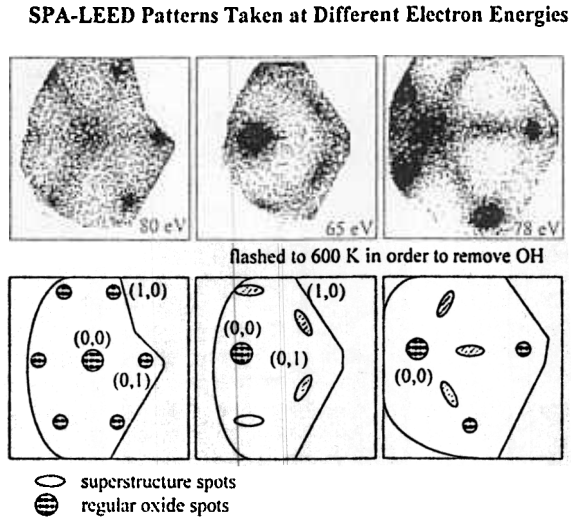

Fig. 10: SPA-LEED patterns of NiO(111)/Ni(111).

arrangement shown in the left hand side of Fig. 9 yields an electrostatic potential energy which increases linearly with the number of oxide layers thereby leading to divergence of the Madelung potential energy. A way out is to reduce the charge in the top and the bottom layers of the polar oxide film by 50 % as shown in the right hand side of Fig. 9. In this case the potential energy is independent of the number of layers. Reduction of the charge density may be achieved by a reduction of the number of surface ions, by a reduction of the charge of the surface ions, by a reconstruction which effectively reduces the charge in the surface region or by a charged adsorbate which makes up a layer with a charge density of 50 % of that of the oxide bulk layers. The latter two cases occur for NiO(111)/Ni(111).

We have studied the structure the NiO(111)/Ni(111) surface with a highly

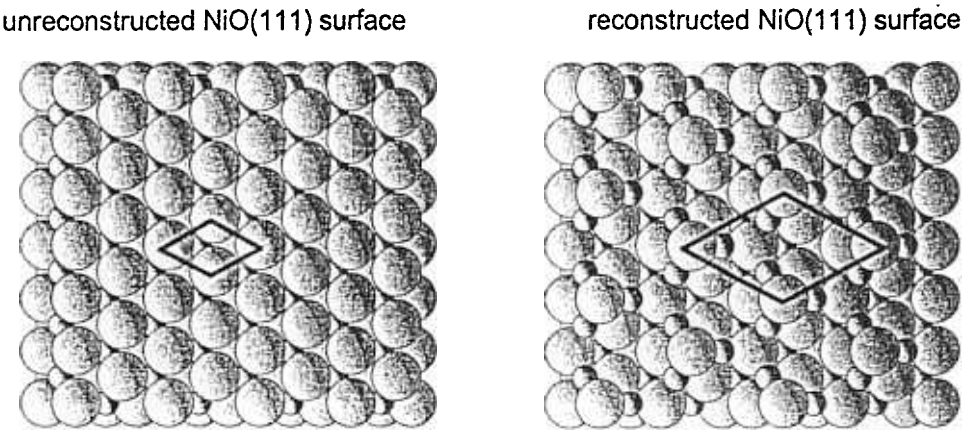

Fig. 11: Structure of unreconstructed polar NiO(111) with O^{2-} termination (left panel) and a surface with an oxygen terminated octopolar reconstruction (right panel).

sensitive LEED system equipped with a channel plate detector [24]. For a clean, freshly flashed NiO(111) film diffuse extra reflexes at (2x2) positions are observed (Fig. 10). This is in line with a theoretical result obtained by Wolf [36]. He calculated the energy of several differently terminated NiO(111) surfaces and found that a so called octopolar reconstruction should have the lowest surface energy [36]. This reconstruction leads to a (2x2) superstructure in the LEED pattern and is shown in the right panel of Fig. 11 in comparison with an unreconstructed surface. The surface energy of the (2x2) reconstruction is comparably low because it consists of octopolar units (4 ions of each type) which exhibit only an octupole field but no dipole field.

NiO(111) shows a high affinity towards the interaction with water [58]. The water in the residual gas atmosphere of the UHV chamber induces the formation of a ELS signal of hydroxyl groups within several minutes whereas NiO(100) seems to be much less active towards water dissociation [58]. The reason for the high activity of the NiO(111) surface gets clear upon studying LEED intensity profiles of the oxide (Fig. 12) [24]. One observes that the (2x2) spots of the octopolar reconstruction are extinguished upon prolonged interaction with the residual gas atmosphere which means that the surface structure changes upon coverage by hydroxyl groups. When the hydroxyl groups are removed by annealing at 600 K the (2x2) reflexes are restored. The explanation for this

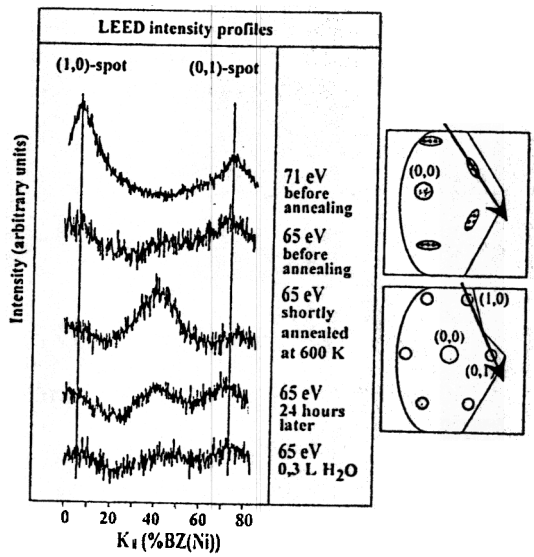

Fig. 12: SPA-LEED line scans of the NiO(111)/Ni(111) surface taken for different preparation conditions.

result is that the Madelung potential energy of the polar NiO(111) surface may also be stabilized by a charged adsorbate layer. Assuming that the formal charge of the hydroxyl ions is -1 which is half of that of the oxide ions, a dense layer of OH^- groups should be able to stabilize the surface so that the octopolar reconstruction that is observed for the clean surface is no longer needed. Another conclusion is that the energy of the adsorbate covered unreconstructed surface must be smaller than that of the reconstructed surface since otherwise one would not observe such a high affinity towards the dissociation of water.

Using TDS experiments with NO we could show that part of the oxide film prepared by oxidation of Ni(111) consist of regions which expose (100)

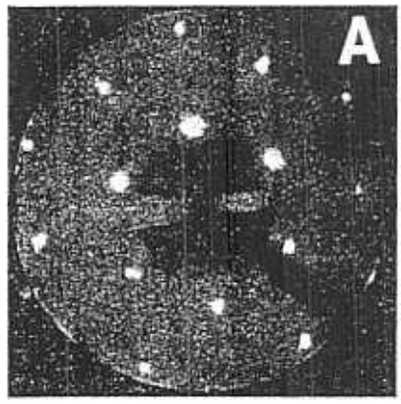

Fig. 13: LEED pattern of clean Au(111). E=127 eV.

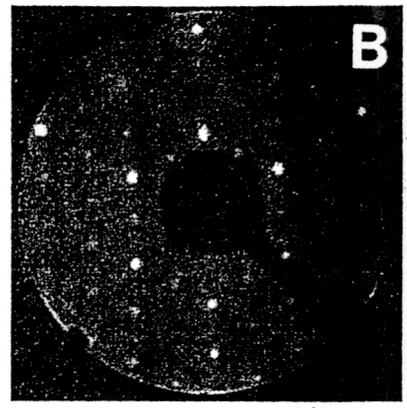

Fig. 14: LEED pattern of p(2x2) reconstructed NiO(111) grown by deposition of ≈3 ML of Ni in an oxygen atmosphere of $\approx 2*10^{-6}$ mbar onto a Au(111) crystal held at T=300 °C.

oriented surfaces to the vacuum [58]. This leads to NO desorption spectra which are very similar to those observed for NiO(100)/Ni(100) and to a certain degree of similarity of the electronic excitation spectra of both surfaces as observed with ELS.

NiO(111) may also prepared by evaporation of Ni in an oxygen atmosphere onto an Au(111) substrate [16,17]. Contrary to the case of NiO(111)/Ni(111)

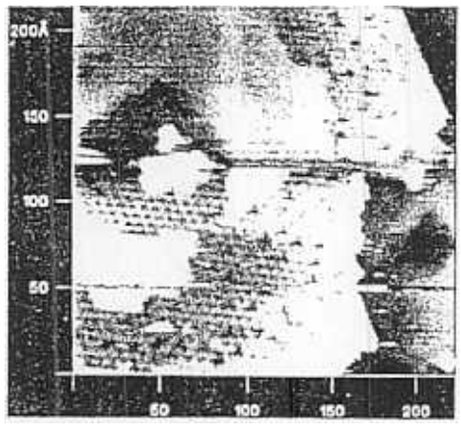

Fig. 15: 250x250 Å^2 STM image of p(2x2) NiO(111)/Au(111). V_s=-5 V, I=0.5 nA.

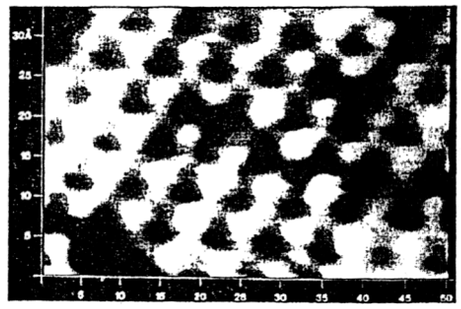

Fig. 16: 35x50 Å^2 STM image of p(2x2) NiO(111)/Au(111). V_s=-5V, I=0.5 nA.

there is only a small lattice mismatch in this case which leads to a smaller number of defects. The preparation of the oxide layer is achieved by evaporation of ≈3 ML of Ni in an oxygen atmosphere of $\approx 2*10^{-6}$ mbar onto an Au(111) substrate held at a temperature of T=673 K. LEED patterns of uncovered Au(111) and NiO(111)/Au(111) are depicted in Fig. 13 and Fig. 14 [16, 17]. As discussed before for NiO(111)/Ni(111) the polar structure of the oxide film is stabilized by an octopolar reconstruction leading to a p(2x2) superstructure in the LEED pattern which is well developed for the NiO(111) film on Au(111). Two STM scans of the oxide layer are depicted in Fig. 15 and Fig. 16 [16, 17]. In the large scale image (Fig. 15) p(2x2) reconstructed regions are observed together with relatively flat regions where no atomic resolution could be achieved. The reconstructed region exhibits several missing-atom defects. In the STM scan also a step between two p(2x2) reconstructed regions is observed. The step height is 2.4 Å which indicates that on both terraces the reconstructed surface is terminated by the same ion. A STM scan of a smaller region of the surface is depicted in Fig. 16. Here tripod like structures seem to emanate. This observation fits well to the model of the reconstructed surface as developed by Wolf [36] and presented in Fig. 11.

3.1.2 Electronic structure

The electronic structure of NiO has been studied in the past by several groups using theoretical as well as experimental methods [59]. As a result it is possible today to model the electronic properties of this oxide with a high degree of accuracy using ab initio cluster calculations. Here we will concentrate on results obtained for NiO(100)/Ni(100) and NiO(111)/Ni(111).

3.1.2.1 Bandstructure of NiO(100)/Ni(100)

NiO(100) was one of the first ionic systems where the bandstructure was accurately determined [34, 53]. One of the questions regarding the electronic structure concerned the nature of the electron states of NiO. Two experimentally determined bandstructures are shown in Fig. 17 [34]; one of NiO(100) cleaved in vacuo and one of NiO(100)/Ni(100). These bandstructures were determined under the assumption that the final state is a free electron like parabolic band with an inner potential of 3.5 eV and an effective mass of $1*m_e$. Another experimentally determined bandstructure has been published by Shen et al. [53] It is obvious that the two bandstructures shown in Fig. 17 are similar which means that the electronic structure of the film is near to that of the single crystal surface. The bandstructure of the thin NiO(100) film appears to be shifted to

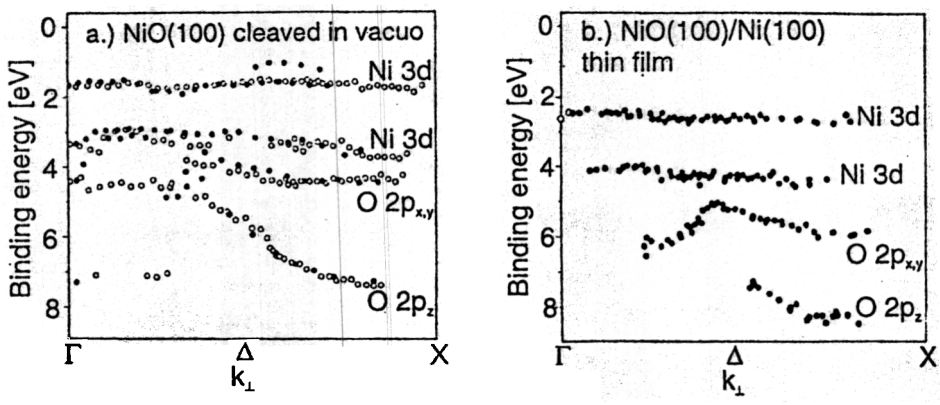

Fig. 17: Bandstructures of cleaved NiO(100) (left panel) and NiO(100)/Ni(100) (right panel).

somewhat lower energy, which is due to defects contained in the film. The upper two non dispersing bands are due to Ni^{2+} ionizations whereas the other bands which show strong dispersions have to be attributed to the 2p levels of the O^{2-} ions.

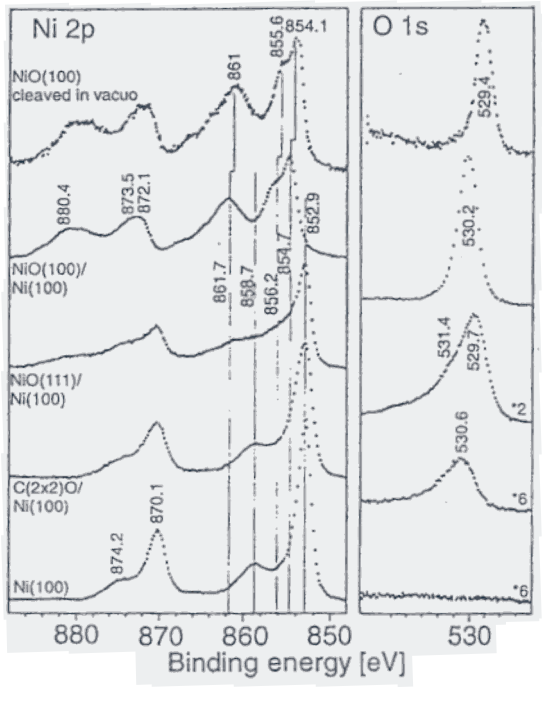

Fig. 18: Ni 2p and O 1s core level spectra of clean Ni(100), oxygen covered Ni(100), NiO(100)/Ni(100), and NiO(100) cleaved in vacuo.

From this observation one may conclude that the Ni^{2+} electronic states are localized (small dispersion) whereas the O^{2-} bands are delocalized (dispersion of some electron volts). This is what is expected from chemical intuition for an oxide like NiO since the charge transfer from Ni to O in the oxide leads to an occupation of spatially extended states of the oxygen ions whereas the outer valence states of the Ni ions are unoccupied in the oxide. This has certain consequences for the photoelectron spectra of the Ni^{2+} ions. Due to the localized nature of the electronic states correlation effects and, in particular hole localization have to be taken into account. For NiO this leads to complicated photoionization spectra with intense shake up lines which are partly under discussion even today [43]. The satellite lines are found in the valence level region as well as in the energetic regime of the core levels [34, 48, 50].

As an example a set of core level spectra is shown in Fig. 18 [34]. The

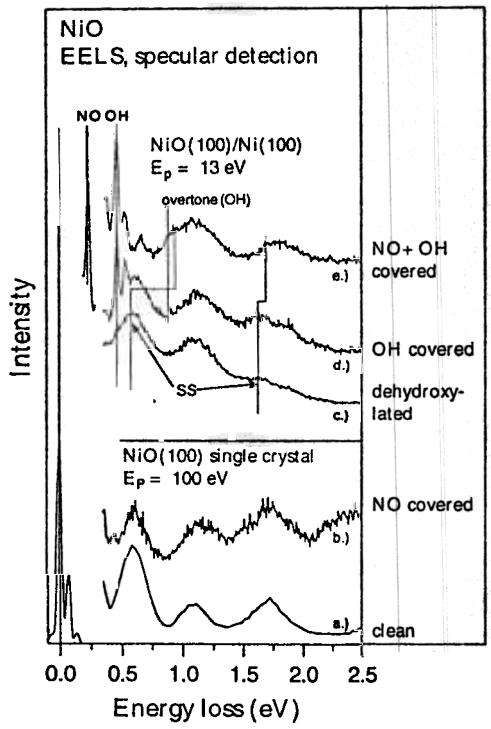

Fig. 19: ELS spectra of a dehydroxylated, an OH covered and a NO+OH covered film of NiO(100) on Ni(100). At the bottom spectra of a clean and a NO covered NiO(100) single crystal surface are shown.

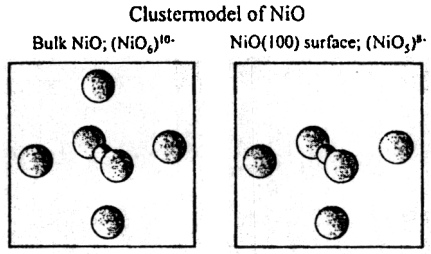

Fig. 20: Arrangement of ions used to model NiO in the bulk (left panel) and the (100) surface (right panel).

spectra shall not be discussed in detail, but it is obvious that the ones of the Ni 2p levels are more complex for NiO than for Ni which is to be attributed to the localization of the Ni^{2+} electronic states in NiO. Similar to the case of the valence bands we observe a shift to higher binding energy in the core level regime of NiO(100)/Ni(100) as compared to NiO(100). However, the general structure of the spectra is the same.

3.1.2.2 Electronic excitations

The study of electronic excitations with ELS turns out to be very fruitful for oxides with a sufficiently large bandgap and a partially filled valence band of the metal ions [23, 55, 56, 58, 63-66]. If these conditions are fulfilled one may detect energy losses in the region of the optical gap which are due to electronic transitions within the valence band of the metal ions. Since such transitions are optically forbidden or only weakly allowed they tend to be not very intense but, due to the resulting long lifetime their halfwidth is usually small so that even complicated systems with complicated excitation functions may be studied. The small intensity turns out to be unproblematic since the background intensity in the optical gap is very small.

A set of ELS spectra of NiO(100)/Ni(100) is shown in the upper part of Fig. 19 [58]. One observes intense and sharp losses due to vibronic excitations at energies below 0.6 eV and somewhat broader features at higher energies due to electronic transitions within the 3d manifold of the Ni^{2+} ions. Two of the latter losses are due to surface excitations as concluded from their sensitivity towards NO adsorption and spin resolved ELS experiments [55]. These losses are marked (SS) in Fig. 19. OH ions on the surface do not modify these excitations which indicates that the hydroxyl groups must be coordinated to non regular sites on the surface. The spectra of the NiO(100) crystal cleaved in vacuo look similar. However, the effect of NO adsorption is not as pronounced as in the case of the NiO(100) film. This is most likely due to an incompleteness of the NO layer which we attribute to insufficient cooling or to desorption due to the electron beam. Cooling is always a problem for massive single crystals like the one used for these experiments.

The electronic surface excitations are local sensors for the electronic and geometric structure of the surface as well as for the geometry of adsorbates and their interaction with the surface since their energy depends strongly on the local surrounding. Therefore the electronic excitation spectrum of the NiO(100) surface and NiO in the bulk has been theoretically modelled using ab initio calculations. For these calculations clusters as shown in Fig. 20 have been used.

In order to model the electric fields correctly these clusters were surrounded by an infinite array of point charges (bulk) or a semi infinite array (surface). Additionally, calculations have been performed for a NO molecule bound to a nickel ion at the surface using a $(NiO_5\text{-}NO)^{8-}$ cluster with the NO molecule tilted by different angles with respect to the surface normal. Since we were only interested in the excitations of the Ni^{2+} ions it was sufficient to explicitly model the first coordination shell of this ion and to replace the other ions by point charges. The results of the calculations (MC-CEPA formalism; except for $(NO\text{-}NiO_5)^{8-}$ (VCI(d))) are presented in Fig. 21 in comparison with the experimental

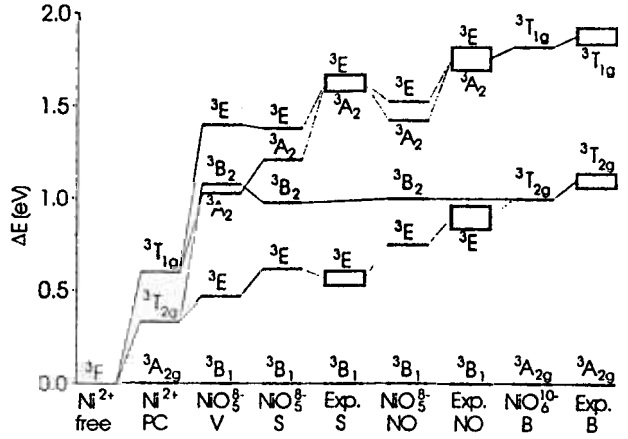

Fig. 21: Comparison of experimental data with theoretical calculation for the lowest electronic excitations of a Ni^{2+} ion in different surroundings. Ni^{2+} (PC): Ni^{2+} surrounded by an infinite array of point charges. NiO_5^{8-} (V): Ni^{2+} near to an oxygen vacancy. NiO_5^{8-} (S): Ni^{2+} at the surface. Exp. (S): Experimentally determined excitation energies of the surface states. NiO_5^{8-} (NO): ON-NiO_5^{8-}. Exp. (NO): Experimentally determined excitation energies for the NO covered surface. NiO_6^{10-} (B): Ni^{2+} in the NiO volume. Exp. (B): Experimentally determined excitation energies for Ni^{2+} in the volume.

data.

The results exhibit good agreement between theory and experiment. In order to get information about the NO-NiO(100) bonding different bonding geometries for the NO molecule have been calculated. The best agreement between theory and experiment was achieved for a NO molecule tilted by 45° with respect to the surface normal, bonding via the N-end to the Ni^{2+} ion which agrees with results of a previous study of NO adsorption on NiO(100) where the molecular orientation has been studied with NEXAFS [34]. This shows that the electronic excitation spectrum of metal ions in oxides is well suited to elucidate

details of the interaction with adsorbates. Of course, also information about the local surrounding of the metal ions may be derived. An example will be presented for the Cr_2O_3(0001)/Cr(110) system.

3.2 Cr_2O_3(0001)/Cr(110)

A thin film of Cr_2O_3(0001) may be grown on Cr(110) by thermal oxidation [64-76]. This is usually done by annealing the Cr(110) sample in 10^{-6} mbar of

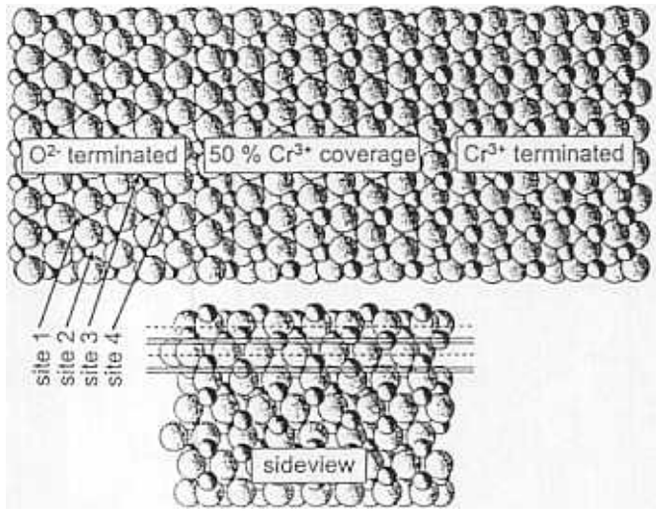

Fig. 22 Different possible terminations of a Cr_2O_3(0001) surface. A sideview with the different chromium and oxygen layers indicated is given at the bottom. Different possible sites of Cr ions on the surface are indicated.

O_2 at about 600 K with subsequent flashing to about 1000 K. This procedure is repeated until the quality of the LEED pattern indicates a well ordered surface. The films prepared this way have a typical thickness of about 50 to 100 Å. The lattice of the oxide fits well to that of the substrate in one direction whereas in the other direction the misfit is pronounced. Therefore especially very thin films show defects which lead to elongated spots in the LEED pattern [76]. The elongation is less pronounced for thicker films.

The (0001) surface of Cr_2O_3 is, like the (111) surface of NiO, polar. Therefore it is again necessary to discuss the stabilization of the surface. As typical for polar surfaces there are different possible surface terminations even

if one neglects reconstruction. These terminations are shown in the left and the right hand side of the upper panel of Fig. 22. Both of them are unstable for energetic reasons. A stable termination is shown in the center. Here half of the Cr ions are missing leading to a surface layer with a charge density reduced by 50 % with respect to that of the bulk layers. Of course, this is not the only possible stable termination. It might also be the case that the surface is reconstructed or that the charges of the surface ions are reduced to some extent. Therefore it was near at hand to start studies with the goal of determining the structure of the $Cr_2O_3(0001)$ surface.

A series of LEED patterns taken at different temperatures is shown in Fig. 23

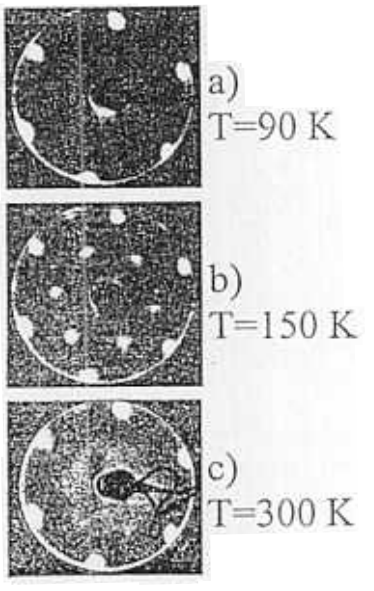

Fig. 23: Series of LEED patterns of $Cr_2O_3(0001)/Cr(110)$ taken at different temperatures.

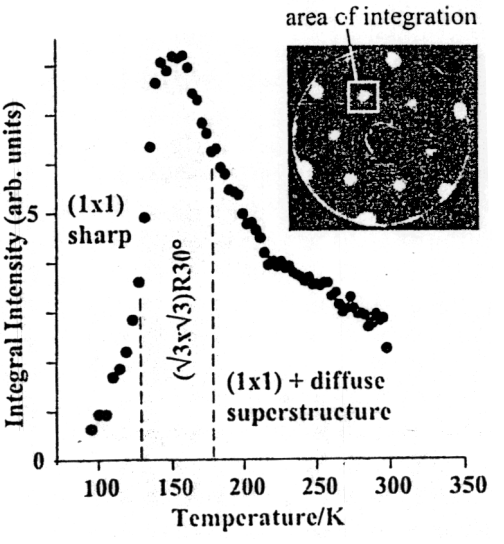

Fig. 24: Intensity of the $(\sqrt{3}x\sqrt{3})R30°$ reflexes as a function of temperature.

[70]. At 90 K a hexagonal pattern as expected for this surface is observed. At 150 K a $(\sqrt{3}x\sqrt{3})R30°$ pattern appears which disappears upon warming up to room temperature. Only some weak and diffuse intensity remains at the $(\sqrt{3}x\sqrt{3})R30°$ positions. The annealing procedure may be repeated with the same result indicating that the process is reversible. From these observations it is obvious that a phase transition occurs at the surface upon changing the temperature.

The intensity of the $(\sqrt{3}x\sqrt{3})R30°$ spots has been recorded as a function of temperature as depicted in Fig. 24 [70]. The maximum of intensity is found at a

temperature of about 150 K whereas at 90 K the intensity is near to zero. This means that at 90 K and 150 K the ordering of atoms at the surface must be different. Starting from T=150 K the intensity decreases smoothly with some weak and diffuse rest intensity remaining even at room temperature (see Fig. 23). This may be explained as thermally induced disorder; i.e. a order-disorder phase transition whereas the phase transition at low temperature is an order-order transition.

Additional information may be derived from ELS data as shown in Fig. 25 [64, 70]. In this figure the transitions within the Cr3d manifold are recorded as a function of temperature. It has been shown previously that the excitations marked A, B, and C are due to chromium ions located at the surface [64, 70]. As is obvious from Fig. 25 the features A and B get weaker when the temperature

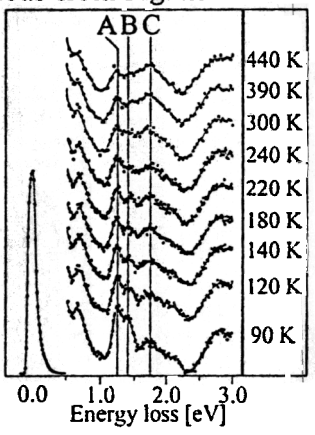

Fig. 25: ELS spectra of Cr_2O_3(0001)/Cr(110) taken as a function of temperature. E_p=100 eV.

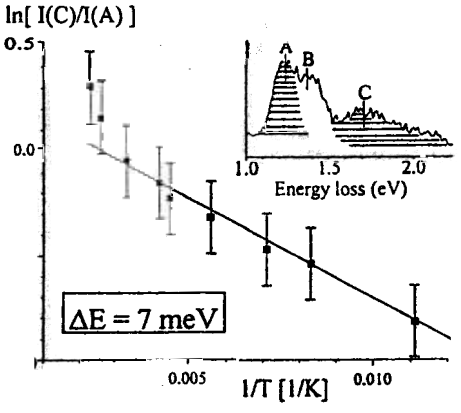

Fig. 26: Logarithm of the intensity ratio of peaks C and A in Fig. 25 as a function of the inverse temperature (Arrhenius plot).

is increased whereas peak C gets more intense. The excitations energies of the Cr ions are very sensitive towards a change of their local surrounding as concluded from adsorption experiments (will be disussed later). Therefore the observed intensity change may be interpreted as to be due to a movement of chromium ions on the surface during the phase transition. Specifically, the chromium ions move from a site characterized by the features A and B to a site characterized by peak C when the temperature is increased.

The temperature dependent changes of the intensities of the surface excitations may be used to calculate the energy difference between the two chromium sites on the surfaces via an Arrhenius plot where the logarithm of the intensity ratio of peaks C and A is drawn as a function of the reciprocal temperature as shown in Fig. 26. From the slope of the curve the energy

difference between the sites may be estimated to be about 7 meV. However, the curve is not fully linear. This may mean that the surface was not always in its thermal equilibrium which is not unlikely since especially at low temperature site hopping of the chromium ions is frozen in as concluded from LEED experiments using low currents in the nA range [71]. Additionally it has to be considered that a phase transitions occurs at the surface which means that an evaluation via the Arrhenius formula is only allowed in the limit of a small coherence length of the transition. However, the coherence length will most likely not be too large due to defects in the structure of the surface.

To get some more detailed information on the structure of the clean surface

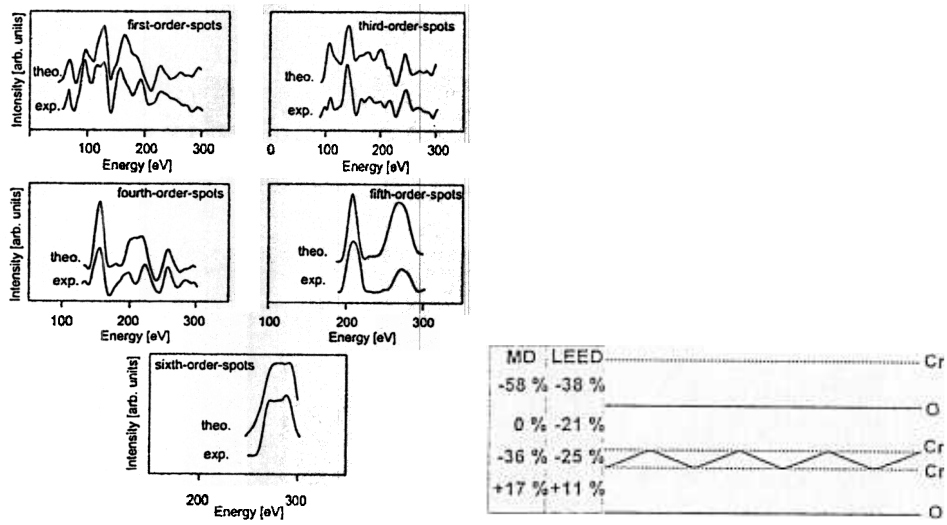

Fig. 27: Left panel: LEED I/V curves for different reflexes of Cr_2O_3(0001)/Cr(110) in comparison with calculated curves. Right panel: modification of some layer-layer spacings in the surface region of Cr_2O_3(0001)/Cr(110) as derived from LEED experiments and molecular dynamics calculations.

LEED intensity measurements have been performed [71]. A set of I/V curves in comparison with theoretically modeled curves obtained by calculations using the tensor LEED program package is depicted in Fig. 27. These data reveal that at low temperature only site 2 is occupied so that the excitations A and B in Fig. 25 must be due to chromium ions on this site. The data also show that the layer-layer spacing in the surface region is strongly modified as depicted in the right hand side of Fig. 27. These experimental results are corroborated by molecular dynamics simulations which also identify site 2 as the most stable one and also yield strong modifications of the interlayer spacings at the surface

which are given in Fig. 27 [71]. With ab initio theory the d-d excitation energies have been calculated for chromium ions in site 2 for the geometry obtained from the LEED experiments and the molecular dynamics calculations yielding values of 0.75, 1.10, 1.30, 1.40 eV and 0.99, 1.25, 1.42, 1.62 eV, respectively. Both sets of values fit reasonably well to the experimental excitation energies of 1.24 and 1.40 eV for the peaks A and B in Fig. 25. We will come back to the topic of electronic excitations later in this chapter.

Putting together the information one reaches at a model for the phase transition as depicted in Fig. 28. At low temperature only site 2 is occupied and

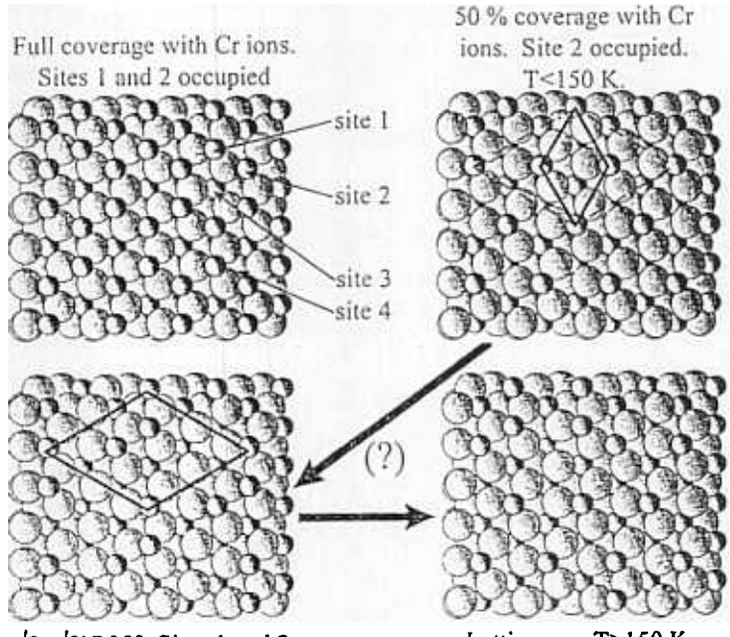

Fig. 28: Model for the phase transitions on Cr_2O_3(0001)/Cr(110).

the density of Cr ions at the surface is only 50 % of the that in the bulk layers so that the film is energetically stable. Site 2 is a site which is also occupied in the bulk. The unit cell is the small one drawn in the right upper panel of Fig. 28. Upon increasing the temperature part of the chromium ions moves to another site which has arbitrarily been chosen to be site 1 in Fig. 28. This one is also occupied in the bulk. As calculated using full ionic pair potentials the surface energies for the sites 1 to 4 are 4.36, 1.60, 6.34 and 2.69 Jm^{-2} [71], respectively so that site 4 is another candidate that has to be considered.

The unit cell at T=150 K is the one plotted in the lower left panel of Fig. 28 and $(\sqrt{3}x\sqrt{3})R30°$ reflexes appear in the LEED pattern. Further increase of the temperature leads to a statistical occupation of the surface sites; a so called lattice gas forms. This results in diffuse intensity in the LEED pattern around the $(\sqrt{3}x\sqrt{3})R30°$ positions.

The driving force for this transition is not fully understood yet. One point to mention is that Cr_2O_3 is antiferromagnetic with a Neèl temperature of 308 K [77]. Of couse, the transition temperature may be smaller at the surface so that it could be the case that the observed phase transition is driven by a magnetic phase transition at T=150 K at the surface. In this context we note that the intensity of the $(\sqrt{3}x\sqrt{3})R30°$ reflexes is small; only 1 % of the intensity of the main reflexes. This could mean that the phase transition occurs only in special regions of the surface which may, for instance, be very well ordered or contain a special type of defect. However, it could also be the case that the $(\sqrt{3}x\sqrt{3})R30°$ unit cell is induced by an antiferromagnetic ordering of spins so that no site

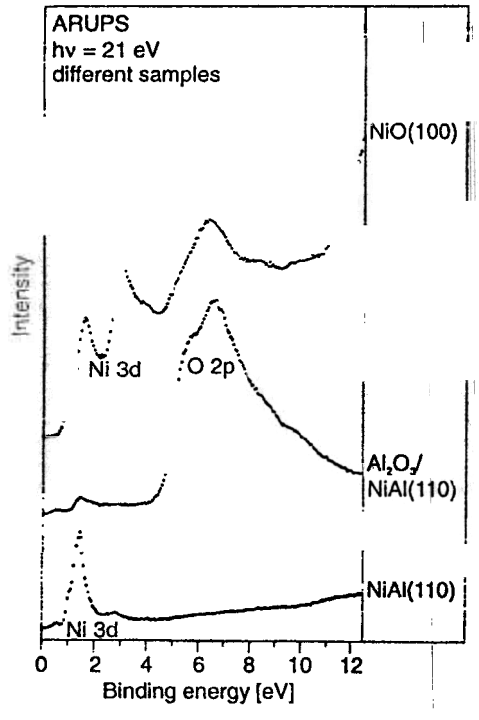

Fig. 29: Comparison of valence photoelectron spectra of NiO(100), Al_2O_3/NiAl(110) and NiAl(110).

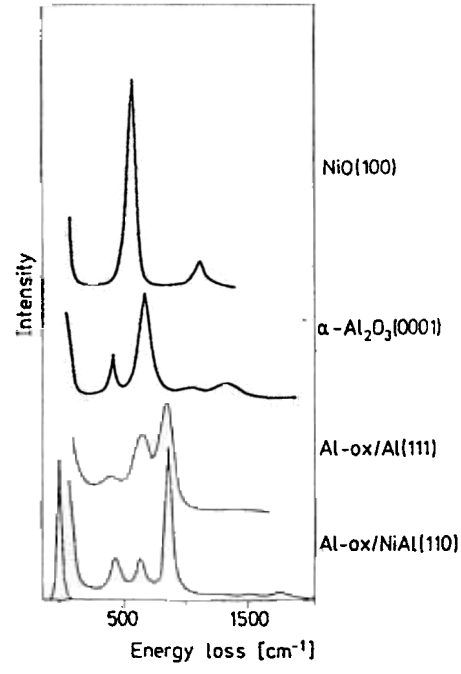

Fig. 30: HREELS spectra of different oxides.

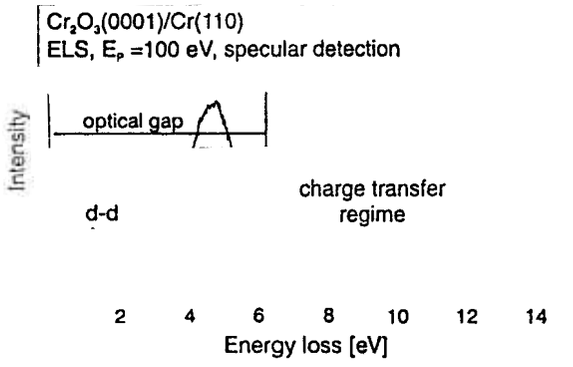

Fig. 32: ELS spectrum of Cr_2O_3(0001)/Cr(110).

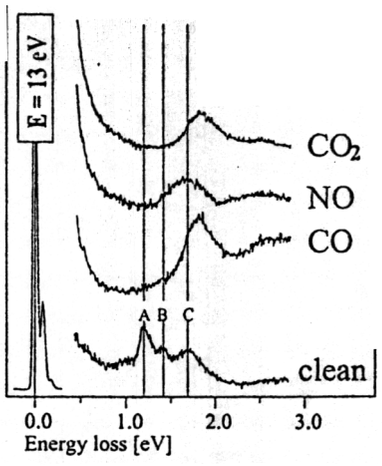

Fig. 33: ELS spectra of clean and adsorbate covered Cr_2O_3(0001).

hopping of the ions at the surface is involved. Investigations on this topic will be performed in near future.

At this point we come back to the electronic excitations of the chromium oxide film. An overview of an ELS spectrum is presented in Fig. 32. At energies between about 1 and 2 eV the already discussed d-d excitations of the chromium ions are found. The intensity in this part of the spectrum is mostly due to excitations occurring at the surface. This gets obvious when spectra of the oxide surface with different adsorbates on it are compared with a spectrum

State	Ideal[1]	LEED[2]	LEED[3]	LEED[4]	MD[5]	Experiment
$^4A_1$	0.88	0.70	0.88	0.86	0.99	0.8
^4E	0.92	1.10	1.21	1.20	1.25	1.2
^4E	1.48	1.30	1.60	1.58	1.42	1.4
$^4A_2$	1.67	1.68	1.60	1.60	1.62	1.8

of an uncovered surface as done in Fig. 33. As expected for surface excitations it is found that the adsorbates modify the d-d excitations strongly.

The excitations of the clean $Cr_2O_3(0001)$ surface have been the topic of calculations [70, 72] The latest theoretical values for the excitations energies of the 4 excitations at lowest energy are given in table 1 [72]. Especially the values determined for the geometry as derived from the LEED experiments fit well to the experimental values. The calculations indicate that the covalency of the bonds at the surface is enhanced with respect to the bulk leading to a reduced ionicity of the ions at the surface.

According to McClure [78] the smallest energy needed for a O->Cr charge transfer excitation is 6.2 eV which is also the energy of the optical gap. These excitations are clearly visible in Fig. 32 at energies above the optical gap. However, there is a intense feature between 4 and 5 eV in the optical gap which might also be a charge transfer excitation as indicated by its intensity and peak form. ELS spectra of adsorbate covered chromium oxide surfaces clearly show that this feature is a surface transition [64, 70]. Therefore one may infer that this feature is due to a charge transfer excitation occuring at the surface of the oxide which would mean that the optical gap at the surface is smaller than that in the bulk. This excitation has also been treated theoretically in ref. [72] using the CASSCF formalism. It could be shown that the energy of the first charge transfer excitation at the surface should be, depending on the nature of the state, between 3.22 and 4.5 eV. As this state would be one in the low energy onset of the loss peak this result fits well to the experimental data thereby pointing towards a reduced width of the optical gap at the surface.

3.3 $Al_2O_3(111)/NiAl(110)$

A thin film of Al_2O_3 may be formed on NiAl(110) by thermal oxidation [11, 79-93]. This is achieved by annealing in $2.5*10^{-6}$ mbar of oxygen at T=500 K for 10 minutes with subsequent flashing to 1100 K. As revealed by Auger data the film thickness is only about 5 Å [92].

A valence photoelectron spectrum of the oxide is presented in Fig. 29 in comparison with spectra of NiO(100) and NiAl(110) [11]. The spectrum of the oxide is dominated by the intense emission of the O2p levels. Besides this only a weak emission near to the Fermi edge shows up which may be attributed to emission from the substrate as revealed by a comparison with the spectrum at the bottom. The emission of Ni^{2+} ions is located in the binding energy range from 1 eV to 3 eV (see spectrum at the top). In the spectrum of the o xide film on NiAl(110) no emission is found in this energy range which could be

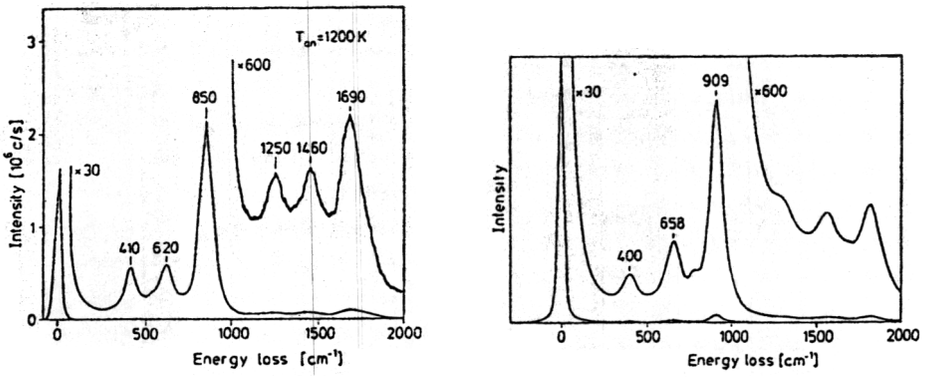

Fig. 31: Left panel: HREELS spectrum of Al_2O_3/NiAl(110). Right panel: calculated HREELS spectrum of γ-Al_2O_3/NiAl(110).

attributed to Ni^{2+} ions so that one may conclude that the oxide film grown on NiAl(110) consists of aluminum oxide.

This result is not too surprising since the formation of aluminum oxide is thermodynamically favorable due to its much higher energy of formation. A similar conclusion may be drawn from the data shown in Fig. 30. A comparison of the HREELS spectra shows that the oxide formed on NiAl(110) is not NiO(100) nor α-Al_2O_3(0001). However, the spectrum of the oxide film is rather similar to that of oxidized aluminum. More detailed information may be derived from Fig. 31 where a HREELS spectrum of Al_2O_3/NiAl(110) is compared to a spectrum calculated for γ-Al_2O_3/NiAl(110) using dielectric theory. The similarity is striking which means that the structure of the oxide film is at least

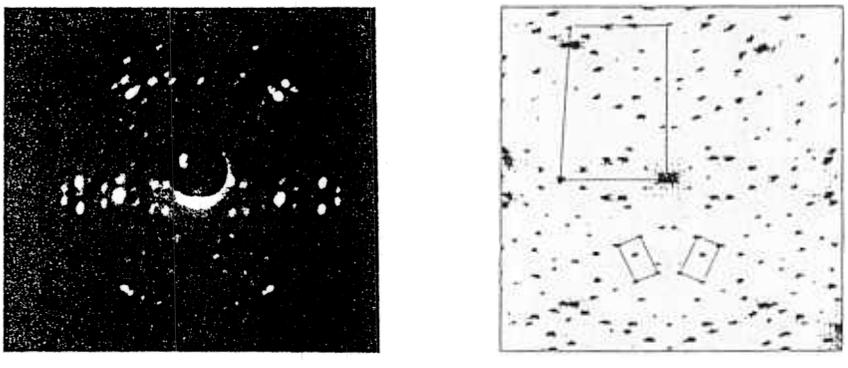

Fig. 34: Left panel: photograph of a LEED pattern of Al_2O_3/NiAl(110). Right panel: SPA-LEED pattern of γ-Al_2O_3 on NiAl(110). The Brillouin zone of the substrate and those of the two domains of the oxide are indicated. Due to aberrations of the SPA-LEED systems the Brillouin zone of the oxide appears is somewhat distorted.

near to that of γ-Al_2O_3. There are some differences between the energetic positions of the losses which is mainly due to the fact that the oxide film was prepared using $^{18}O_2$ instead of $^{16}O_2$.

At this point details of the structure still have to discussed. One hint towards this topic comes from the LEED pattern of the film as shown in Fig. 34. The pattern of the oxide exhibits numerous sharp reflexes. As may be seen from Fig. 34 the Brillouin zone of the film is small and appro ximately rectangular. Two domains of the oxide which are rotated with respect to each other contribute to the LEED pattern. The unit cell as calculated from the LEED pattern has a size of 10.6 Å x 17.9 Å and is commensurate with the substrate only along [001].

In the photograph of the LEED pattern (Fig. 34 left panel) the distribution of intensities of the LEED spots resembles a hexagonal pattern. This is a first sign that the base structure of the oxide is hexagonal. However, the lattice structure

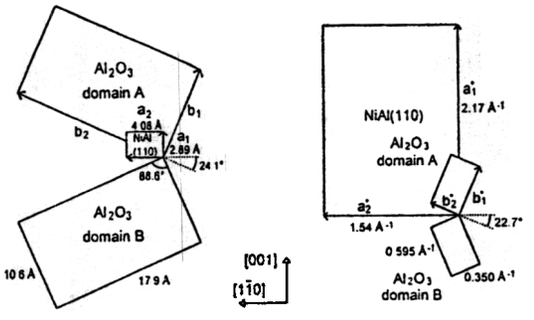

Fig. 35: Schematic diagram exhibiting the Brillouin zones and unit cells of Al_2O_3/NiAl(100) and NiAl(110).

must be somewhat distorted since otherwise one would observe a purely hexagonal pattern for the oxide film instead of the numerous reflexes.

In order to elucidate the structure of the oxide film further studies with electron microscopy have been undertaken [93]. For these studies a crystal with a conical hole as depicted in Fig. 36 has been used. This sample allowed to investigate the supported oxide film as well as unsupported oxide near to the boundary of the hole in the crystal surface. Thicker layers on NiAl with different structure have been studied by Rühle and Coworkers [94].

Before oxidation the hole was drilled into the sample in a system that contained a strong ion gun. The sample was oxidized in a standard UHV chamber where the quality of the oxide film could be judged with LEED. From there the sample was transferred into the electron microscope which was operated at pressures in the 10^{-7} mbar range. During these transfers the sample

had contact with air. However, the oxide film survived the transfers as will be discussed in the following.

Two electron micrographs are shown in Fig. 37; one of the supported oxide and another one of the unsupported film. The micrograph of the unsupported film exhibits several line patterns which are due to planes in the oxide lattice. In table 2 the experimentally determined periods of the line patterns are compared

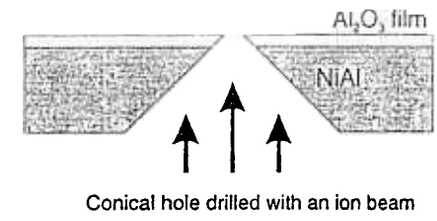

Fig. 36: Schematic diagram of a cut through a NiAl(110) single crystal with oxide film used for the experiments with electron microscopy.

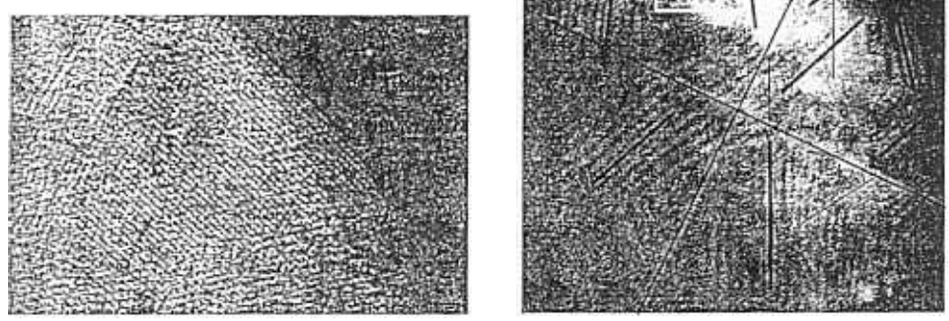

Fig. 37: Left panel: electron micrograph of unsupported Al_2O_3 grown on NiAl(110) (33.6x22.0 nm) In the upper right part of the image aluminium oxide with NiAl(110) support is visible. Right panel (bottom): electron micrograph of supported Al_2O_3/NiAl(110) (84.8x83.5 nm). Right panel (top): section of the micrograph below. (21.9x17.3 nm)

to distances in the lattice of Al_2O_3/NiAl(110) as calculated from the LEED pattern in Fig. 34. This comparison strongly indicates that the structure of the unsupported oxide film is the same than that of the supported film. The same conclusion may be drawn from a fourier transform of part of electron

LEED reflex	Distances in Al_2O_3/NiAl(110) as calculated from the LEED pattern in Fig. 34 [Å]	Distances between lines in the electron micrograph [Å]
$(\bar{1},7)$	2.49	2.45
(0,5)	3.57	3.59
(1,3)	5.24	5.28
$(2,\bar{2})$	4.59	4.57

Table 2: Comparison of lattice spacings in γ-Al_2O_3 with line spacings in the electron micrograph of the unsupported aluminum oxide film.

micrograph (see Fig. 38) as shown in Fig. 37 (left panel) which compares well to the reciprocal space pattern of the oxide film.

The observation that the unsupported film has the same structure than the supported one is interesting by itself. A structure like that of Al_2O_3/NiAl(110) is unique among the numerous modifications of aluminum oxide indicating that the structure of the film is stabilized by the substrate-oxide interaction. Therefore one would expect that the film changes its structure upon removal of the substrate. This is obviously not the case, so that one is led to the conclusion that the structural transformation of the oxide structure into a more stable one is thermodynamically hindered.

In the micrograph of the supported film (Fig. 37, right panel) the lines due to the lattice of the oxide are not observed although the lattice of the substrate is well resolved (top of the right hand side of Fig. 37) However, one observes

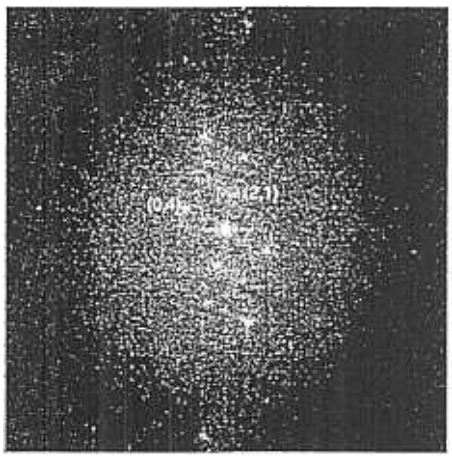

Fig. 38: Fourier transform of part of the electron micrograph shown in Fig. 37 (left panel). The assignment of two maxima to LEED reflexes of Al_2O_3/NiAl(110) is given in the figure.

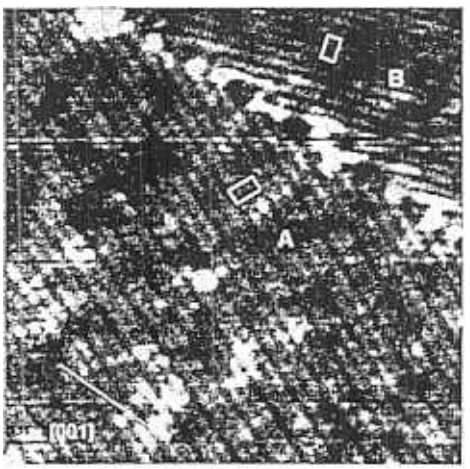

Fig. 39: STM image of Al_2O_3/NiAl(110). CCT, 4 V, 0.5 nA, ≈300x300 Å^2.

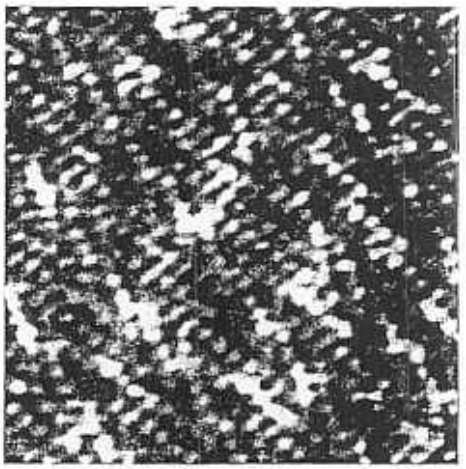

Fig. 40: STM image of Al_2O_3/NiAl(110). CCT, -1 V, 1.5 nA, ≈90x90 Å^2.

broad lines in the micrograph which are oriented in different directions (bottom of the right hand side of Fig. 37). These lines are not due to the lattice of the oxide or the substrate but to both of them. They result from electrons which are scattered first by the substrate and then by the oxide film so that the wave vector change of these electrons corresponds to the sum of a substrate and an oxide lattice vector. When the lengths of the vectors are similar and when they are oriented in nearly opposite directions then the sum of these vectors may be small which corresponds to a large period in real space. This is what is observed in the micrograph of the supported oxide. The experimentally observed lines may be traced back to sums of k-vectors of NiAl(110) and the oxide film.

The directions of the lines are indicated in the right hand side of Fig. 37 (bottom). One finds two types of line systems; i.e. one with a larger spacing (marked with thick black lines) and another one with a smaller spacing (marked with thin black lines). Whereas the first system is due to a (2,0) type beam of the NiAl(110) substrate which is subsequently scattering by the oxide layer the other one is due to a (1,1) type reflex of the substrate, also with subsequent scattering by the oxide. As expected from the symmetry of the system, the $[1\bar{1}0]$ and [001] directions of the substrate act as mirrors lines for the line patterns in that for every line pattern another one is found with a mirrorlike direction.

It was not possible yet to achieve atomic resolution in STM pictures of this oxide. This is at least partly due to the electronic structure of aluminum oxide. Since the bandgap of aluminum oxide is large, voltages of several electron have to be applied to extract electrons from or to put electrons into the oxide. This

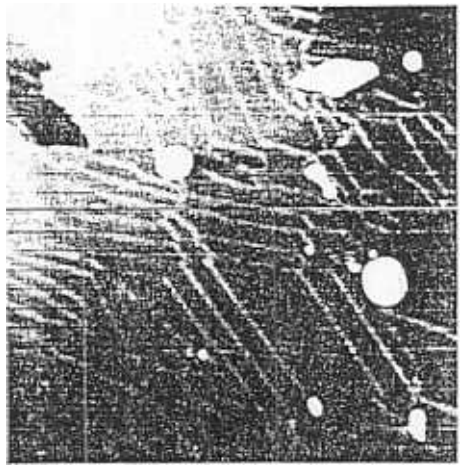

Fig. 41: STM image of Al_2O_3/NiAl(110). CCT, -8 V, 0.5 nA, ≈2400x2400 Å^2.

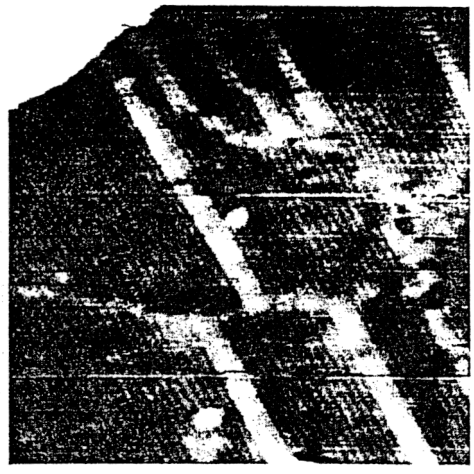

Fig. 42: STM image of Al_2O_3/NiAl(110). CCT, 4 V, 0.5 nA, ≈500x500 Å^2.

corresponds to large tip-surface distances and therefore to a decreased resolution. In Fig. 39 a STM scan taken with a voltage of 4 eV is shown which exhibits a boundary between two oxide domains [83]. At this voltage the oxide seems to be already visible since the oxide unit cells are readily observable (denoted A and B). At low tunneling voltage (1 V) the STM pattern looks different (Fig. 40). Since the oxide has no electronic levels at 1 eV or below the visible structures must be due to the substrate. In this context Fig. 40 shows the first layer of the substrate below the oxide with atomic resolution. A more detailed evaluation of the scan shows that the structure of this layer is distorted due to the interaction with the oxide film.

The structure of the oxide film on a larger scale is depicted in Fig. 41. In this figure antiphase domain boundaries between oxide islands are visible as white lines. Fig. 42 depicts these domains on a larger scale. The reasons for these domains is most likely stress within the oxide film which breaks it into anntiphase domains with an approximate size of 120 Å along [1 $\bar{1}$ 0]. The domain structure can also be observed with SPA-LEED where a splitting of some of the oxide reflexes is observed [83].

4. SUMMARY

In this chapter we have reviewed the properties of some oxide films focusing on preparation, structure and electronic properties. We have shown that the study of oxidic film may be an alternative to single crystal oxides, especially

when electron spectroscopic investigations are concerned. One main topic was the stabilization of polar surfaces which has been discussed for Cr_2O_3(0001)/Cr(110) and NiO(111)/Ni(111) where different stabilization mechanism, including reconstruction and stabilization by a charged adsorbate layer occur. Also, structural investigations using different methods have been discussed for several oxide films. Another topic was the electronic structure of the films with a strong focus on electronic excitations within the valence band of the metal ions. We have shown that these excitations may serve as sensors for the local environment of the ions thereby giving access to informations like the site of the metal ions and their interaction with adsorbates.

ACKNOWLEDGEMENTS

We are grateful to the large number of coworkers who contributed to the results presented here and to the funding institutions which made our work possible. Specifically we name the Deutsche Forschungsgemeinschaft (DFG), the Bundesministerium für Bildung und Forschung (BMBF), the Fonds der Chemischen Industrie (FCI) as well as the European Community (EC).

REFERENCES

1. P. A. Cox, Transition Metal Oxides: An Introduction to their Electronic Structure and Properties, Clarendon Press, Oxford 1992
2. V. E. Henrich and P. A. Cox, *The Surface Science of Metal Oxides*, Cambridge University Press, Cambridge 1994
3. K. Wandelt, Surf. Sci. Rep. **2** (1982) 1
4. H.-J. Freund and E. Umbach (Ed), *Adsorption on Ordered Surfaces of Ionic Solids and Thin Films*, Springer Series in Surface Science, Vol. 33, Springer, Heidelberg 1993
5. H. H. Kung, *Transition Metal Oxides: Surface Chemistry and Catalysis*, Elsevier, Amsterdam 1989
6. M. Bäumer, J. Libuda, H.-J. Freund, *Chemisorption and Reactivity on Supported Clusters and Thin Films: Towards an Understanding of Microscopic Processes in Catalysis*, Nato Adv. Study Institute, Erice, Italy, NATO ASI Series, Kluwer Academic Press 1997
7. H.-J. Freund, Angewandte Chemie, in press (1997)
8. A. A. Davydov, *Infrared Spectroscopy of Adsorbed Species on the Surface of Transition Metal Oxides*, Wiley Interscience, New York 1990
9. S. Witzel, PhD thesis, University of Osnabrück, Osnabrück 1993
10. H.-J. Freund, H.Kuhlenbeck, V. Staemmler, Rep. Prog. Phys. **59** (1996) 283
11. R. M. Jaeger, H. Kuhlenbeck, H.-J. Freund, M. Wuttig, W. Hoffmann, R. Franchy, H. Ibach, Surf. Sci. **259** (1991) 235
12. U. Bardi, A. Atrei, G. Rovida, Surf. Sci. **268** (1992) 87
13. P. J. Chen, D. W. Goodman, Surf. Sci. Lett. **312** (1994) L767

14. Y. Wu, H. S. Tao, E. Garfunkel, T. E. Madey, N. D. Shinn, Surf. Sci.**336** (1995) 123
15. Y. Wu, E. Garfunkel, T. E. Madey, Surf. Sci.**365** (1996) 337
16. H. Hannemann, C. A. Ventrice Jr., Th. Bertrams, A. Brodde, H. Neddermeyer, Phys. Stat. Sol. A **146** (1994) 289
17. C. A. Ventrice Jr., Th. Bertrams, H. Hannemann, A. Brodde, H. Neddermeyer, Phys. Rev. B **49** (1994) 5773
18. W.-D. Wang, P. A. Thiel, J. Chem. Phys. **92**, (1990) 2025
19. M. Bäumer, D. Cappus, G. Illing, H. Kuhlenbeck, H.-J. Freund, J. Vac. Sci. Technol. A **10** (1992) 2407
20. H. Kuhlenbeck, H.-J. Freund in *Adsorption and Reaction of Small Molecules on Oxide Surfaces* in *Springer Proceedings in Physics* **73** (1993) 227
21. St. Uhlenbrock, Chr. Scharfschwerdt, M. Neumann, G. Illing, H.-J. Freund, J. Phys.: Cond. Matter **4** (1992) 7973
22. H.-J. Freund, B. Dillmann, D. Ehrlich, M. Haßel, R. M. Jaeger, H. Kuhlenbeck, C. A. Ventrice, F. Winkelmann, S. Wohlrab, C. Xu, Th. Bertrams, A. Brodde, H. Neddermeyer J. Mol. Catal. **82** (1993) 143
23. A. Freitag, V. Staemmler, D. Cappus, C. A. Ventrice, K. Al-Shamery, H. Kuhlenbeck, H.-J. Freund, Chem. Phys. Lett. **210** (1993) 10
24. F. Rohr, K. Wirth, J. Libuda, D. Cappus, M. Bäumer, H.-J. Freund, Surf. Sci. Lett.**315** (1994) 2977
25. D. Cappus, M. Haßel, E. Neuhaus, F. Rohr, H.-J. Freund, Surf. Sci.**337** (1995) 268
26. J. Klinkmann, D. Cappus, H.-J. Freund, J. Electr. Spectr. Rel. Phen.**72** (1995) 37
27. D. Cappus, J. Klinkmann, H.-J. Freund, Surf. Sci. Lett.**325** (1995) L421
28. G. Dalmai-Imelik, J. C. Bertolini, J. Rousseau, Surf. Sci.**63** (1977) 67
29. H. Conrad, G. Ertl, J. Küppers, E. E. Latta, Sol. Stat. Commun.**17** (1975) 497
30. M. Prutton, J. A. Walker, M. R. Welton-Cook, R. C. Felton, J. A. Ramsey, Surf. Sci.**89** (1979) 95
31. M. Prutton, F. P. Netzer, J. Phys. C. Solid State Phys.**8** (1975) 2401
32. C. G. Kinniburgh, J. A. Walker, Surf. Sci.**63** (1977) 274
33. M. R. Welton-Cook, M. Prutton, J. Phys. C. Solid State Phys.,**13** (1980) 3993
34. H. Kuhlenbeck, G. Odörfer, R. Jaeger, G. Illing, M. Menges, Th. Mull, H.-J. Freund, M. Pöhlchen, V. Staemmler, S. Witzel, C. Scharfschwerdt, K. Wennemann, T. Liedke, M. Neumann, Phys. Rev. B **43** (1991) 1969
35. M. Schönnenbeck, D. Cappus, J. Klinkmann, H.-J. Freund, L. G. M. Pettersson, P. S. Bagus, Surf. Sci., submitted
36. D. Wolf, Phys. Rev. Lett. **68** (1992) 3315
37. A. Freitag, V. Staemmler, to be published
38. R. Lacmann, Colloq. Int. CNRS **152** (1965) 195
39. A. Freitag, PhD thesis, University of Bochum, Bochum 1995
40. V. Staemmler in *Adsorption on Ordered Surfaces of Ionic Solids and Thin Films*, Springer Series in Surface Science **33**, ed H.-J. Freund and E. Umbach, Springer, Heidelberg 1993
41. M. A. Nygren, L. G. M. Pettersson, J. Electron Spectrosc. Relat. Phenom.**69** (1994) 43
42. L. G. M. Pettersson, Theor. Chim. Acta **87** (1994) 293
43. A. Fujimori, T. Saitoh, T. Mizokawa, A. E. Bocquet, Jap. J. Appl. Phys. Suppl. **32-3** (1993) 217

44. J. Freitag, V. Staemmler, J. Electron Spectrosc. Relat. Phenom. **69** (1994) 99
45. M. Pöhlchen, V. Staemmler, J. Chem. Phys. **97** (1992) 2583
46. N. R. Rösch, K. M. Neymann, U. Birkenheuer, in *Adsorption on Ordered Surfaces of Ionic Solids and Thin Films*, Springer Series in Surface Science **33**, ed H.-J. Freund and E. Umbach, Springer, Heidelberg 1993
47. N. U. Zhanpeisov, A. G. Pelmenschikov, G. M. Zhidomirov, Kinet. Catal. **31** (1990) 563
48. G. J. M. Janssen, W. C. Nieuwpoort, Phys. Rev. B **38** (1988) 3449
49. P. S. Bagus, G. Pacchioni, F. Parmigiani, Chem. Phys. Lett. **207** (1993) 569
50. A. Fujimori, F. Minami, Phys. Rev. B **30** (1984) 957
51. F. Manghi, C. Calandra, S. Ossicini, Phys. Rev. Lett. **73** (1994) 3129
52. R. S. Saiki, A. P. Kaduwela, J. Osterwalder, C. S. Fadley, C. R. Brundle, Phys. Rev. B **40** (1989) 1586
53. Z.-X. Shen, C. K. Shih, O. Jepsen, W. E. Spicer, I. Lindau, J. W. Allen, Phys. Rev. Lett. **64** (1990) 2442
54. S. Hüfner, G. Wertheim, Phys. Rev. B **8** (1973) 4857
55. B. Fromme, M. Möller, Th. Anschütz, C. Bethke, E. Kisker, Phys. Rev. Lett. **77** (1996) 1548
56. A. Gorschlüter, H. Merz, Phys. Rev. B **49** (1994) 17293
57. P. A. Cox, A. A. Williams, Surf. Sci. **153** (1985) 791
58. D. Cappus, C. Xu, D. Ehrlich, B. Dillmann, C. A. Ventrice Jr., K. Al-Shamery, H. Kuhlenbeck, H.-J. Freund, Chem. Phys. **177** (1993) 533
59. M. Bäumer, D. Cappus, H. Kuhlenbeck, H.-J. Freund, G. Wilhelmi, A. Brodde, H. Neddermeyer, Surf. Sci. **253** (1991) 116
60. R. W. G. Wyckoff, *Crystal Structures*, 2nd edition, Wiley Interscience, New York 1965
61. J. W. Tasker, J. Phys. C: Solid State Physics **12** (1979) 4977
62. J. W. Tasker, Phil. Mag. A **39** (1979) 119
63. H. Kuhlenbeck, Appl. Phys. A **59** (1994) 469
64. H. Kuhlenbeck, C. Xu, B. Dillmann, M. Haßel, B. Adam, D. Ehrlich, S. Wohlrab, H.-J. Freund, U. A. Ditzinger, H. Neddermeyer, M. Neuber, M. Neumann, Ber. Bunsenges. Phys. Chem. **96** (1992) 15
65. M. Haßel, H. Kuhlenbeck, H.-J. Freund, S. Shi, A. Freitag, V. Staemmler, S. Lütkehoff, M. Neumann, Chem. Phys. Lett. **240** (1995) 205
66. H. Kuhlenbeck, M. Bäumer, M. Bender, D. Cappus, B. Dillmann, D. Ehrlich, F. Rohr, M. Schönnenbeck, O. Seiferth, H.-J. Freund in *Elementary Processes in Excitations and Reactions on Solid Surfaces*, ed A. Okiji, K. Makoshi, Springer Series in Solid State Sciences **121**, Springer, Heidelberg 1996
67. C. Xu, M. Haßel, H. Kuhlenbeck, H.-J. Freund, Surf. Sci. **258** (1991) 23
68. C. Xu, B. Dillmann, H. Kuhlenbeck, H.-J. Freund, Phys. Rev. Lett. **67** (1991) 3551
69. C. A. Ventrice, D. Ehrlich, E. L. Garfunkel, B. Dillmann, D. Heskett, H.-J. Freund, Phys. Rev. B **46** (1992) 12892
70. M. Bender, D. Ehrlich, I. Yakovkin, F. Rohr, M. Bäumer, H. Kuhlenbeck, H.-J. Freund, V. Staemmler, J. Phys: Cond. Matter **7** (1995) 5289
71. F. Rohr, M. Bäumer, H.-J. Freund, J. A. Mejias, V. Staemmler, S. Müller, L. Hammer, K. Heinz, Surf. Sci. Lett., in press (1997)
72. J. A. Mejias, V. Staemmler, H.-J. Freund, submitted
73. A. Stierle, P. Bödecker, H. Zabel, Surf. Sci. **327** (1995) 9

74. H. M. Kennett, A. E. Lee, Surf. Sci. **33** (1972) 33
75. P. Michel, C. Jardin, Surf. Sci. **36** (1973) 478
76. S. Ekelund, C. Leygraf, Surf. Sci. **40** (1973) 179
77. J. B. Goodenough, Prog. Solid State Chem. **5** (1972) 145
78. D. S. McClure in *Electronic States of Inorganic Compounds: Experimental Techniques*, ed P. Day, Reidel, Dordrecht 1975
79. M. Wuttig, W. Hoffmann, R. Jaeger, H. Kuhlenbeck, H.-J. Freund, Mat. Res. Soc. Symp. Proc. **221** (1991) 143
80. R. M. Jaeger, H. Kuhlenbeck, H.-J. Freund, Chem. Phys. Lett. **203** (1993) 41
81. R. M. Jaeger, J. Libuda, M. Bäumer, K. Homann, H. Kuhlenbeck, H.-J. Freund, J. Electron Spectrosc. Relat. Phenom. **64** (1993) 217
82. J. Libuda, M. Bäumer, H.-J. Freund, J. Vac. Sci. Technol. A **12** (1994) 2259
83. J. Libuda, F. Winkelmann, M. Bäumer, H.-J. Freund, Th. Bertrams, H. Neddermeyer, K. Müller, Surf. Sci. **318** (1994) 61
84. S. Wohlrab, F. Winkelmann, H. Kuhlenbeck, H.-J. Freund, *Adsorption on Epitaxial Oxide Films as Model Systems for Heterogeneous Catalysis*, Springer Proceedings in Physics, accepted
85. Th. Bertrams, F. Winkelmann, Th. Uttich, H.-J. Freund, H. Neddermeyer, Surf. Sci. **331** (1995) 1515
86. J. Libuda, A. Sandell, M. Bäumer, H.-J. Freund, Chem. Phys. Lett. **240** (1995) 429
87. M. Bäumer, J. Libuda, A. Sandell, F. Winkelmann, H.-J. Freund, G. Graf, Th. Bertrams, H. Neddermeyer, Ber. Bunsenges. Phys. Chem. **99** (1995) 1381
88. A. Sandell, J. Libuda, P. Bruhwiler, S. Andersson, M. Bäumer, A. Maxwell, N. Mårtensson, H.-J. Freund, J. Vac. Sci. Technol. **14** (1996) 1546
89. A. Sandell, J. Libuda, P. Bruhwiler, S. Andersson, M. Bäumer, A. Maxwell, N. Mårtensson, H.-J. Freund, J. Electron Spectrosc. Relat. Phenon. **76** (1995) 301
90. J. Doychak, J. L. Smialek, T. E. Mitchell, Metall. Trans. A **20** (1989) 499
91. K. Müller, H. Lindner, D. M. Zehner, G. Ownby, Verh. Dtsch. Phys. Ges. **25** (1990) 1130
92. H. Isern, G. R. Castro, Surf. Sci. **211/212** (1989) 865
93. M. Klimenkov, S. Nepijko, H. Kuhlenbeck, H.-J. Freund, in preparation
94. J. C. Yang, E. Schumann, H. Mullejans, M. Rühle, J. Phys. D: Appl. Phys **29** (1996) 1716